On the Evolution of the Skeleton

Jonas August
Yale University
Department of Electrical Engineering

Allen Tannenbaum
University of Minnesota
Department of Electrical Engineering

Steven W. Zucker
Yale University
Departments of Computer Science
and Electrical Engineering

Abstract

It is commonly held that skeleton variation due to noise is unmanageable. It is also believed that smoothing, invoked to combat noise, creates no new structures, as in the causality principle for smoothing images. We demonstrate that both views are incorrect. We characterize how smooth points of the skeleton evolve under a general boundary evolution, with the corollary that, when the boundary is smoothed by a geometric heat equation, the skeleton evolves according to a related geometric heat equation. The surprise is that, while certain aspects of the skeleton simplify, as one would expect, others can behave wildly, including the creation of new skeleton branches. Fortunately such sections can be flagged as ligature, or those portions of the skeleton related to shape concavities. Our analysis also includes junctions and an explicit model for boundary noise. Provided a smoothness condition is met, the skeleton can often reduce noise. However, when the smoothness condition is violated, the skeleton can change violently, which, we speculate, corresponds to situations in which "parts" are created, e.g., when the handle appears on a rotating cup.

1 Introduction

When the boundary of an object evolves in time, how does its skeleton change? It is commonly held that this classical shape descriptor is unstable to boundary perturbations. This is important because, although rapid object recognition would seem to require hierarchical shape representations to organize database search, it supports the view that such hierarchies cannot be computed reliably (Fig. 1). As a remedy, smoothing is often believed to reveal a simpler underlying structure that is obscured by noise. While such operations, formulated using heat equations [11], were engineered to satisfy a causality principle, their success has led to the widespread view that smoothing never creates new structures (Fig. 1 and Movies[1] 1 and 2). We show that both views are incorrect. By analyzing how the skeleton changes as a function of boundary changes, the foundations for a stability theory are laid. By considering the different types of structure involved, we can articulate the objects to which causality principles may be applied.

We begin by characterizing how smooth points of the

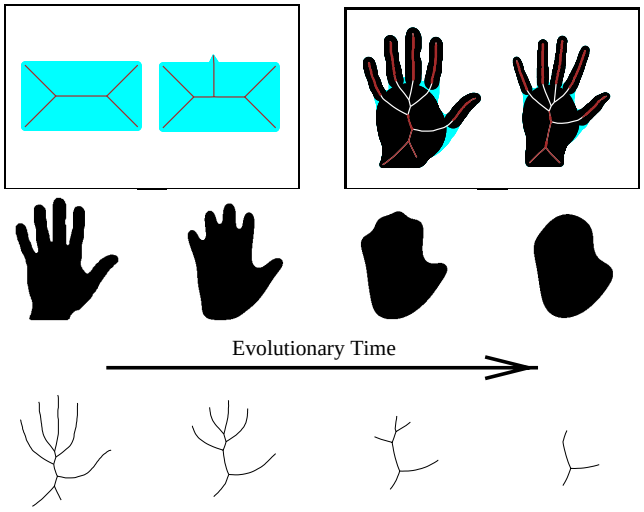

Figure 1: How the skeleton changes due to boundary variation. (TOP ROW) The Bad News: the instability of the skeleton. (LEFT BOX) The skeleton (lines) of a rectangle is drastically altered by a small boundary "glitch". (RIGHT BOX) Two objects of similar qualitative shape have distinct skeleton topologies (note the differing branching to the middle fingers, in white), suggesting that skeleton topology cannot be used to define generic shape classes, such as "hand". (MIDDLE ROW) The Good News: boundary simplification via smoothing. The boundary of a hand evolves in time via a geometric heat equation, where the evolutionary time represents the degree of smoothing (view Movie 1). (BOTTOM ROW) At each instant of time the evolved boundary has a corresponding skeleton. Observe that skeleton structures are only removed in this example of boundary smoothing (view Movie 2). Our analysis of how the skeleton evolves as the boundary evolves is the subject of this paper. It suggests not only when "good news" will hold, but also flags the "bad news" situations and stresses the importance of ligature (white skeleton points, TOP RIGHT BOX).

[1] Go to "http://cvc.yale.edu/people/grad_students/August" for movies.

skeleton evolve under a general boundary evolution. A pleasing application of this result is that, when the boundary is smoothed by a geometric heat equation, the skeleton evolves according to a related geometric heat equation. Thus there is a sense in which the skeleton is smoothed as well, and branches shorten, as one might expect (Fig 1, bottom). We calculate several other skeletal properties that behave in this fashion, such as inflection points. The surprise is that, while certain aspects of the skeleton simplify, others can behave rather wildly. For example, we provide instances of skeletal branch lengthening, and of junction creation [16].

While this might at first seem to preclude the use of skeleton-based descriptions, such as shock trees [17] in object recognition, the satisfying aspect of our analysis is that the formulas also show when the skeleton evolution will become singular, and thus provide a way out. Such badly-behaved portions of the skeleton are characterized by ligature, which implies that ligature should be included in the skeleton labeling for recognition [2].

Our analysis also includes junctions and an explicit model for boundary noise. Provided a smoothness condition is met, the skeleton can often reduce noise. However, when the smoothness condition is violated, the skeleton can change violently, which, we speculate, corresponds to situations in which "parts" are created, e.g., when the handle appears on a rotating cup.

2 Skeleton dynamics in general

Consider the boundary of a planar object evolving in time. This gives rise to a family of curves $C(\cdot,t)$, where $t \in \mathbb{R}$ is evolutionary time. Each such curve has a well-defined interior and therefore has a corresponding *skeleton*, which is the set of centers of maximal discs contained inside the curve. The skeleton is composed of branches, each of which is a curve $Q = Q(s,t) \in \mathbb{R}^2$, where $s \in \mathbb{R}$ is the arc-length along the skeleton. Let $r = r(s,t) \in \mathbb{R}$ be the radius of the maximal disc at Q, which touches the boundary of the object at the two (curve) points $C_i = C(s_i,t) \in \mathbb{R}^2$, where $i = 1,2$, and s_i is the arc-length along the boundary at C_i (Fig. 2). Thus we have a family of skeletons $(Q(\cdot,t), r(\cdot,t))$ corresponding to the family of boundaries that record the evolution of the object.

The (unit-length) tangent vectors at Q and C_i are $T = Q' = \frac{\partial Q}{\partial s}$ and $T_i = \frac{\partial C_i}{\partial s_i}$, respectively. The normal vectors N and N_i are $\frac{\pi}{2}$ counter-clockwise rotations of T and T_i, respectively. The orientation of T is θ, and the angle between T and N_i is φ. Notation is summarized in Table 1. In §A, we prove:

Theorem 1 *Let an initial boundary curve $C_i = C(s_i,0)$ be given, where $i = 1,2$ denotes parameterization as in Fig. 2. If the evolution for the boundary is given by:*

$$\dot{C}_i = \nu_i N_i, \tag{1}$$

where $\nu_i = \nu_i(s_i) \in \mathbb{R}$ is the velocity of C_i in its normal direction, then the skeleton Q will evolve as:

$$\dot{Q} = \tau T + \nu N, \tag{2}$$

where τ and ν are the tangential and normal components of the skeleton velocity and:

$$\dot{\varphi} = \frac{\frac{\partial \nu_2}{\partial s_2} - \frac{\partial \nu_1}{\partial s_1}}{2} \tag{3}$$

$$\dot{\theta} = \frac{\frac{\partial \nu_1}{\partial s_1} + \frac{\partial \nu_2}{\partial s_2}}{2} \tag{4}$$

$$\tau = -\frac{r\dot{\varphi}}{\sin\varphi} \tag{5}$$

$$\nu = \frac{\nu_2 - \nu_1}{2\sin\varphi} \tag{6}$$

$$\dot{r} = \tau\cos\varphi - \frac{\nu_1 + \nu_2}{2}. \tag{7}$$

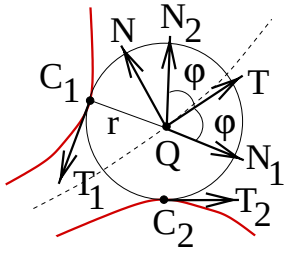

Figure 2: A maximal disc (circle) of radius r at skeleton (dashed curve) point Q touches the boundary (bold curves) at points C_1 and C_2, with tangent and normal vectors (see text). We study how the skeleton point Q evolves as the boundary points C_1 and C_2 evolve.

3 Application to specific evolutions

We now apply Theorem 1 to some important kinds of curve evolution along the boundary.

3.1 Constant motion ($\nu_i = 1$)

Blum's grass-fire, itself a form of curve evolution, can be described mathematically using $\nu_i = 1$, and is known to give rise to shocks [7, 10].

Corollary 1 *Suppose that the boundary evolves via $\dot{C}_i = N_i$. Then the skeleton will evolve as:*

$$\dot{\varphi} = \dot{\theta} = \tau = \nu = 0, \quad \dot{r} = -1.$$

Thus the skeleton point remains fixed but the maximal disc radius r decreases at a constant rate. When the radius becomes 0, the skeleton point Q disappears.

3.2 Curvature motion ($\nu_i = \kappa_i$)

Boundary smoothing can be formulated using $\dot{C}_i = \kappa_i N_i$, the geometric heat equation. The *boundary-axis ratio*[2] $g_i = \mp\frac{\partial s_i}{\partial s} > 0$ is the local ratio of the length of boundary at C_i corresponding to a length of skeleton at Q. The following is proved in §B:

Corollary 2 *The evolution of a skeleton corresponding to a curve undergoing curvature motion satisfies:*

$$\begin{aligned}
\dot{\varphi} &= \frac{\frac{\partial \kappa_2}{\partial s_2} - \frac{\partial \kappa_1}{\partial s_1}}{2} \\
\dot{\theta} &= \frac{\frac{\partial \kappa_1}{\partial s_1} + \frac{\partial \kappa_2}{\partial s_2}}{2} \\
\tau &= -\frac{r\dot{\varphi}}{\sin\varphi} \\
\nu &= \frac{\kappa}{g_1 g_2} \\
\dot{r} &= \tau\cos\varphi - \frac{\kappa_1 + \kappa_2}{2}
\end{aligned}$$

These formulas are important not only because they assure us that in many instances the dynamics of the skeleton are well-behaved, but also because they reveal clues about the origin of unstable behavior of the skeleton. Shaked [16] and Taxiera [18] also derived formulas for skeleton evolution; in addition, Taxiera used catastrophe theory [4] to classify the transitions of the skeleton at singularities.

4 Quantitative results within a branch

As shown in [6], we can reparameterize the skeleton (at smooth points) so that $\tau = 0$. Let $M = (g_1 g_2)^{-1}$; note that M is positive (see (25) in §B). Corollary 2 then implies:

Proposition 1 *When the boundary of an object evolves under the geometric heat equation $\dot{C}_i = \kappa_i N_i$, its skeleton also evolves according to a geometric heat equation $\dot{Q} = \nu N = M\kappa N$, with $M > 0$.*

We now state some of the simplifying properties of the skeleton that this result leads to.

4.1 Length

Let $S(t)$ be a smooth arc of the skeleton at time t with endpoints Q_* and R_*, where R_* is a three-branch junction. These are the generic junctions of the skeleton [19]. Then

$$\begin{aligned}
\frac{d}{dt}\text{length of } S(t) &= -\int_{S(t)} \kappa\nu ds + \text{boundary terms} \\
&= -\int_{S(t)} M\kappa^2 ds + \text{boundary terms.}
\end{aligned}$$

Boundary terms aside, since the integral term is negative, this means that the point Q_* is moving into the skeleton. In §6, we show that a branch can in fact lengthen at junctions.

[2] We adopt the convention henceforth that the top symbol of $\pm$ or $\mp$ refers to the case $i = 1$ and the bottom symbol refers to the case $i = 2$ (for example, $\mp$ denotes $+$ for $i = 2$).

4.2 Scalar parabolic equations

In this section, we apply some results of [1, 13] to study the behavior of some key quantities of the skeleton. In particular, we review some of their results on the zero set of a solution of a scalar parabolic equation of the form:

$$u_t = a(x,t)u_{xx} + b(x,t)u_x + c(x,t)u, \tag{8}$$

where $x_0 < x < x_1, 0 < t < T$, and $u_x = \frac{\partial u}{\partial x}$, etc. We assume that $a, a_x, a_{xx}, b_x, b_t, c$ are continuous on the rectangle $[x_0, x_1] \times [0, T]$, and that $a(x,t)$ is strictly positive. Let u be a classical solution of (8), which we assume is continuous on the rectangle $[x_0, x_1] \times [0, T]$, and such that $u(x_i, t) \neq 0$ for $i = 0, 1$ and $0 \leq t \leq T$. Define the *zero set of u* to be

$$Z(t) = \{x \in [x_0, x_1] : u(t, x) = 0\}.$$

$Z(t)$ is a compact subset of (x_0, x_1). Let $z(t)$ denote the number of elements of $Z(t)$. Then Angenent [1] proves that the number of zeros $z(t)$ *does not increase with time*. This is the key result which we use below.

4.3 Tangent angles

We now compute what happens to the tangent angle θ. Using a proof similar that for (28) [8, 9], we see that: $\frac{\partial\theta}{\partial t} = \frac{\partial\nu}{\partial s} = \frac{\partial}{\partial s}(M\kappa) = \frac{\partial}{\partial s}(M\frac{\partial\theta}{\partial s})$, and thus:

$$\frac{\partial\theta}{\partial t} = M\frac{\partial^2\theta}{\partial s^2} + M_s\frac{\partial\theta}{\partial s}. \tag{9}$$

Thus from [1], the number of zeros of θ is nonincreasing, that is for any line ℓ the number of points on the skeleton $S(t)$ with tangent parallel to ℓ decreases (unless new points with tangent parallel to ℓ are introduced at the endpoints Q_* or R_*).

4.4 Inflection points

We now analyze what happens to the inflection points of the evolving skeleton, that is, points where the curvature vanishes. Using a proof similar to (10) [8, 9], we have:

$$\frac{\partial\kappa}{\partial t} = \frac{\partial^2\nu}{\partial s^2} + \kappa^2\nu = M\kappa_{ss} + 2M_s\kappa_s + (M_{ss} + \kappa^2 M)\kappa.$$

Hence the number of zeros of κ (inflection points) decreases except possibly at the endpoints Q_* and R_* of $S(t)$.

4.5 Singular motions within a branch

Corollary 2 reveals two key classes of pathological skeleton evolution. First, observe that when $\varphi \to 0$, τ and therefore $\dot{r}$ will blow up. This formal instability has been heuristically addressed previously using "velocity-based" methods of pruning the skeleton [14, p. 617]. Second, the normal velocity ν may become singular as well. To understand this, note that $g_1 = g_2$ implies $\kappa_1 = \kappa_2$, using (34). From Theorem 1, we then find that $\nu \to 0$ and $\kappa \to 0$ when

$g_1 = g_2 \to 0$. While this is not a singularity in the skeleton, it is in the boundary: $\kappa_1 = \kappa_2 \to -\infty$. Blum [3] called such portions of skeleton *full ligature*: a non-zero length of skeleton corresponds to exactly two concave corners in the boundary. Full ligature can occur when $\varphi \to 0$ as well, as seen in Fig. 4 and Movie 3. However, if *only one* of g_1 or g_2 approach 0, then $|\nu| \to \infty$. This new pathology occurs when only one boundary is a concave corner ($\kappa_i \to -\infty$); the corresponding piece of skeleton is called *semiligature*. The rapid motion of semiligature in its normal direction is clear in Fig. 4 and Movie 4.

5 Endpoints

This and the next section articulate the behavior of the "boundary terms" referred to in §4.1 (cf. [16, 18]). To study the motion of the skeleton at endpoints, we use the constraint that the maximal disc at the endpoint is the osculating circle[3] of a positive curvature maximum, or $r = 1/\kappa_i$. To find $\dot{r}$, we first observe that $\dot{\kappa}_i = \kappa_i^2 \nu_i + \frac{\partial^2 \nu_i}{\partial s_i^2}$, using (27), (28) and that $\frac{\partial \theta_i}{\partial s_i} = \kappa_i$. We then conclude:

$$\dot{r}_{endpoint} = \frac{\partial}{\partial t}\frac{1}{\kappa_i} = -\nu_i - r^2 \frac{\partial^2 \nu_i}{\partial s_i^2}. \qquad (10)$$

Noting that $\nu_1 \to \nu_2$ and $\varphi \to \pi$ at an endpoint, we use the formula for $\dot{r}$ in Theorem 1 to compute:

$$\tau_{endpoint} = r^2 \frac{\partial^2 \nu_i}{\partial s_i^2}. \qquad (11)$$

To obtain ν at the endpoint, we note that: $\frac{\partial}{\partial s_i}(\nu_2 - \nu_1) \to 0$, given that ν_i is smooth. In addition, using φ' from §B, we find that: $\frac{\partial \varphi}{\partial s_2} = \frac{\partial s}{\partial s_2}\varphi' = (1/g_2)\kappa_2 g_2 = 1/r$. Finally, we use l'Hospital's rule on the formula for ν by differentiating with respect to s_2 to conclude:

$$\nu_{endpoint} = 0. \qquad (12)$$

In the case of the geometric heat equation, where $\nu_i = \kappa_i$, we see that $\tau = r^2 \frac{\partial^2 \kappa_i}{\partial s_i^2} < 0$, since a skeleton endpoint corresponds to boundary curvature maximum. Thus skeleton branches shorten at endpoints under boundary smoothing (Fig. 1 and Movie 2).

6 Junctions

To calculate skeleton motion at junctions, we will consider only the generic 3-branch case shown in Fig. 3, since junctions of four or more branches are unstable [19]. Observe that the maximal disc at a junction contacts the boundary at exactly three points C_i, $i = 1, 2, 3$. Along one of the branches meeting at the junction, 1 say, we fix a coordinate system (T, N). Note that (19) will hold for $i = 1, 2, 3$ at the junction, leading to the following linear system:

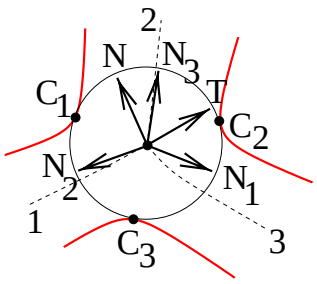

Figure 3: The neighborhood of a three-branch junction of the skeleton.

$$\begin{bmatrix} \nu_1 \\ \nu_2 \\ \nu_3 \end{bmatrix} = \begin{bmatrix} N_1 \cdot T & N_1 \cdot N & -1 \\ N_2 \cdot T & N_2 \cdot N & -1 \\ N_3 \cdot T & N_3 \cdot N & -1 \end{bmatrix} \begin{bmatrix} \tau \\ \nu \\ \dot{r} \end{bmatrix}, \qquad (13)$$

where we solve for skeleton growth ($\dot{r}$) and motion (τ and ν), in terms of boundary motion (ν_i, where $i = 1, 2, 3$).

6.1 Branch lengthening

We now apply this linear system to explain branch lengthening under boundary smoothing. Suppose we have a junction, say a, where normal vectors N_1 and N_3 are parallel but perpendicular to N_2. Suppose the boundary of the object at C_1 and C_3 is flat, but sharply concave at C_2 (Fig. 5 and Movie 5). Substituting into (13), we see:

$$\begin{bmatrix} 0 \\ \kappa_2 \\ 0 \end{bmatrix} = \begin{bmatrix} 0 & -1 & -1 \\ -1 & 0 & -1 \\ 0 & 1 & -1 \end{bmatrix} \begin{bmatrix} \tau_a \\ \nu_a \\ \dot{r}_a \end{bmatrix}, \qquad (14)$$

with the solution $\nu_a = \dot{r}_a = 0, \tau_a = -\kappa_2 \to \infty$. The junction rushes toward C_2 as the curve there rapidly smoothes outward, thus *lengthening* the skeleton branch between C_1 and C_3. This situation is not intuitive, since boundary smoothing mathematically is known to shorten the boundary. Indeed, the geometric heat equation $\dot{C}_i = \kappa_i N_i$ is also called the curve-shortening flow, for among all possible choices of ν_i, $\nu_i = \kappa_i$ causes the length of the boundary to shrink fastest. This result says that although the boundary shortens, individual branches may grow! Note that this occurs near ligature (Fig. 5).

6.2 Unstable 4-branch junctions

A 4-branch junction will generically occur as two nearby 3-branch junctions, say a and b. Let the above configuration be junction a (Eq. (14)). Now introduce another concavity at C_4, near to C_2, and so create another junction b near to a. This describes a three-fingered hand with a narrow middle

[3] Note that the maximal disc only touches the boundary at one point generically at a skeleton endpoint.

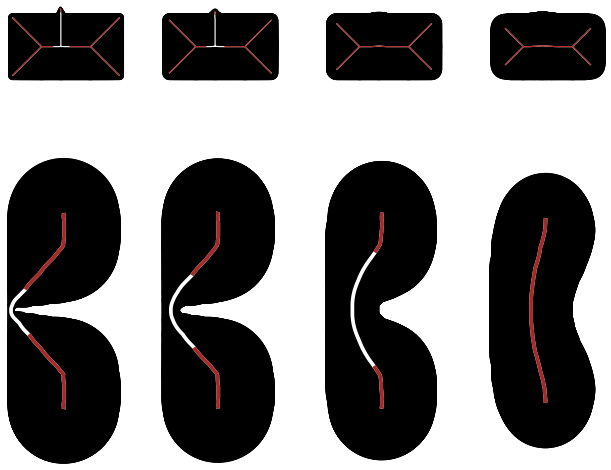

Figure 4: Ligature and singular motions of the skeleton under boundary smoothing. The initial curves bound objects shown in black, and the skeleton for each object is shown in the interior. Shock type [10] is not shown, but ligature (computations are described in [2], using skeletons from [15]) is shown in white. Smoothing is implemented by a curve shortening flow [8] and increases from left to right. (TOP ROW) A boundary glitch with its large corresponding branch (vertical) is flagged by ligature. The glitch is rapidly removed via smoothing, inducing a rapidly changing ligature region (view Movie 3). (BOTTOM ROW) Singular skeleton motion at semiligature. As described in §4.5, the concave corner causes extremely high skeleton normal velocity $\nu = \kappa/(g_1 g_2)$, as seen in the rapid flattening of the skeleton in this semiligature region (view Movie 4).

finger. For junction b, we have:

$$\begin{bmatrix} \kappa_4 \\ \kappa_2 \\ 0 \end{bmatrix} = \begin{bmatrix} \epsilon - 1 & -\epsilon & -1 \\ \epsilon - 1 & \epsilon & -1 \\ 0 & 1 & -1 \end{bmatrix} \begin{bmatrix} \tau_b \\ \nu_b \\ \dot{r}_b \end{bmatrix}, \qquad (15)$$

with solution $\tau_b \approx -(\kappa_4 - \kappa_2)/(2\epsilon) = -\nu_b = \dot{r}_b$, for $\epsilon \to 0$ and $\kappa_2 \neq \kappa_4$. We conclude that $\frac{d}{dt}\text{length}(\overline{ab}) \to \pm|\kappa_4 - \kappa_2|/(\sqrt{2}\epsilon)$: the skeleton branch joining junctions a and b can lengthen or shorten, even causing a change in topology (observe the nearby ligature in Fig. 5b and Movie 6).

7 The stochastic skeleton

Since the motion of the contour C_i depends on the normal motion $\nu_i = \nu_i(s_i)$, we can create a model for shape perturbation by considering ν_i as a random process. Suppose a probability space (Ω, F, P) is given, and $\omega \in \Omega$. View $\nu_i(s_i)$ as a random variable, and $\nu_i(\cdot, \omega)$ as a fixed random function, taking the real value $\nu_i(s_i, \omega)$ at s_i. To simplify notation, we suppress the dependence on ω.

We desire an expression for the random perturbations of the skeleton in terms of those along the boundary. Theorem 1 does this for any fixed $\nu_i(s_i)$, provided ν_i is continuously differentiable. Since ν_i is defined along the closed boundary of the object undergoing evolution, ν_i is periodic with period L, the perimeter of the object, and can be written as the Fourier series $\nu_i(s_i) = \Sigma_{k\in\mathbb{Z}} a_k \exp(j2\pi k s_i/L)$, where $a_k \in \mathbb{R}$ and $j = \sqrt{-1}$. Now, by Theorem 9.4 of [12, p. 33], ν_i will be continuously differentiable if $\Sigma_{k\in\mathbb{Z}}|k||a_k|$ converges, which is true if $a_k = O(\frac{1}{|k|^d})$, as $k \to \pm\infty$, for $d > 2$ (say $d = 3$). Thus the smoothness of ν_i is determined by the rate at which a_k decays as $k \to \pm\infty$. So far, this analysis allows us to generate a suitable ν_i for a given set of numbers a_k.

To introduce randomness, let $\{a_k\}$ be a countable set of random variables whose densities satisfy the above decay rate. In particular, we consider ν_i as a random process, parametrized along the boundary, whose realizations are continuously differentiable and can therefore be used in Theorem 1. It is sufficient to consider a_k with any probability density $p_{a_k} : \mathbb{R} \to \mathbb{R}$ having the following bounded support: $\text{supp}(p_{a_k}) \subset [-b_k, b_k], b_k = O(\frac{1}{|k|^3}), k \in \mathbb{Z}$. With probability one, $a_k = O(\frac{1}{|k|^3}), \forall k$, and thus ν_i is continuously differentiable.

Since the maximal disk at skeleton point Q typically touches the boundary at *distant* points C_1 and C_2, we can assume that ν_1 and ν_2 are practically uncorrelated but identically distributed, as are $\frac{\partial \nu_1}{\partial s_1}(s_1), \frac{\partial \nu_2}{\partial s_2}(s_2)$. (Note that the random process ν_i is constrained primarily at neighboring points because of the high-frequency decay; low frequencies are unconstrained.) Let $\sigma_{\nu_1}, \sigma_{\nu_2}, \sigma_{\frac{\partial \nu_1}{\partial s_1}}, \sigma_{\frac{\partial \nu_2}{\partial s_2}}$ denote the standard deviations of the random variables $\nu_1(s_1), \nu_2(s_2), \frac{\partial \nu_1}{\partial s_1}(s_1), \frac{\partial \nu_2}{\partial s_2}(s_2)$, respectively. We immediately conclude from Theorem 1 that:

Proposition 2 *If $\nu_i(s_i) = \Sigma_{k\in\mathbb{Z}} a_k \exp(j2\pi k s_i/L)$, with a_k independent random variables with support bounded as above, then:* $\frac{\sigma_\varphi}{\sigma_{\frac{\partial \nu_i}{\partial s_i}}} = \frac{1}{\sqrt{2}}$, $\frac{\sigma_\theta}{\sigma_{\frac{\partial \nu_i}{\partial s_i}}} = \frac{1}{\sqrt{2}}$,

$\frac{\sigma_\tau}{\sigma_{\frac{\partial \nu_i}{\partial s_i}}} = \frac{r}{\sqrt{2}\sin\varphi}$, $\frac{\sigma_\nu}{\sigma_{\nu_i}} = \frac{1}{\sqrt{2}\sin\varphi}$, $\sigma^2_{\dot{r}} = \frac{r^2}{2\sin^2\varphi}\sigma^2_{\frac{\partial \nu_i}{\partial s_i}} + \frac{1}{2}\sigma^2_{\nu_i}$.

Under the above assumptions and the perturbation model they imply, this result means that in contrast to the popular belief about the sensitivity of the skeleton to boundary noise, the skeleton can in fact reduce noise. For example, if $\varphi \approx \frac{\pi}{2}$ (parallel sides), the normal motion standard deviation is only about .707 that of the corresponding boundaries. However, also observe that noise amplification in τ, ν, and $\dot{r}$ is possible, even going singular as $\varphi \to 0$. Thus this random model reassures us that the skeleton is generally not sensitive to noise, and flags those instances when it is. Zhu recently proposed a random model of approximate skeletons [20] for characterizing natural shapes.

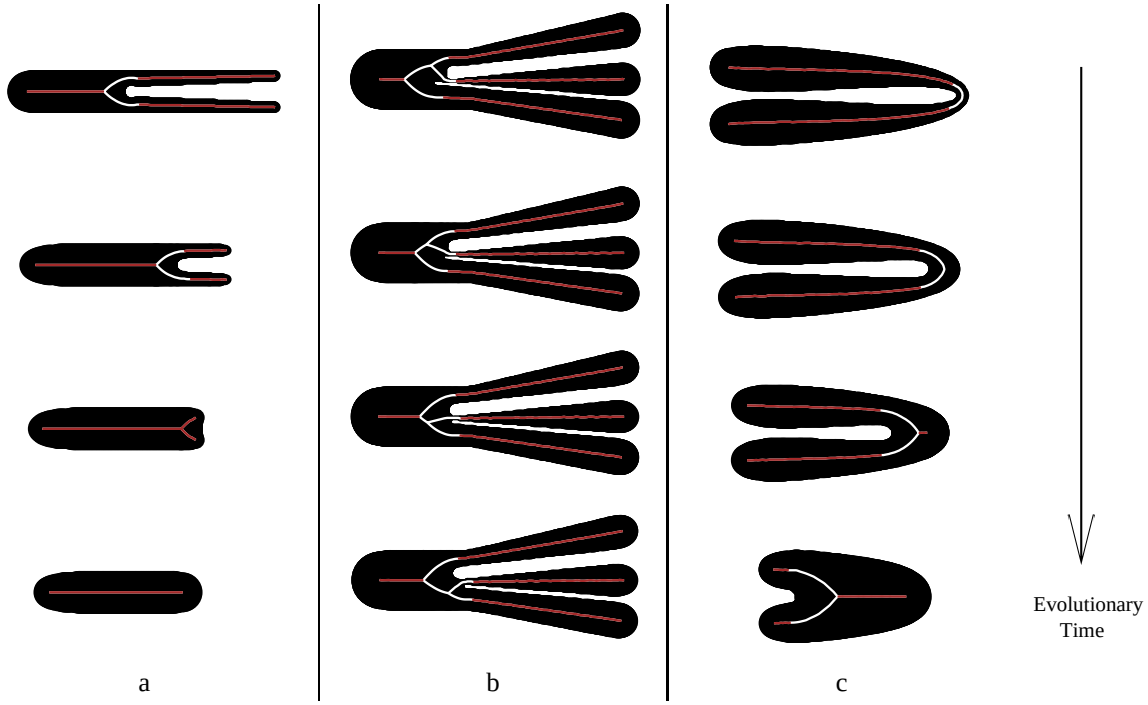

Figure 5: Examples of the evolution of the skeleton under boundary smoothing ($\nu_i = \kappa_i$): wild behavior near ligature (white). (a) From branch lengthening to branch death. A deep concavity in the boundary, which is related to ligature, rapidly rushes rightward under boundary smoothing, causing the left branch to grow, as predicted by (14). Eventually the concavity disappears and later the two rightmost branches are annihilated. (b) Unstable 4-branch junctions. Initially, the top and middle fingers join at the upper 3-branch junction. Under boundary smoothing ($\nu_i = \kappa_i$), this junction momentarily passes through the left 3-branch junction to join the middle and bottom fingers; notice how the instability is signalled by ligature. (c) The non-causality of boundary smoothing. While smoothing is typically invoked to eliminate structure, the geometric heat equation on the boundary induces the birth of a new branch on the right (view Movie 7). $\kappa_i = r^{-1}, i = 1$ or 2 is required for branch birth [16, 18]. Observe that this event emerges out of a ligature region of the skeleton. This is consistent with the use of ligature in part decomposition [2].

If a_k decays slower than $O(\frac{1}{|k|^d})$, for *all* $d > 2$, then ν_i will not be continuously differentiable, and Theorem 1 can hold only in a generalized sense. Discontinuities in ν_i or its derivative may create corners in the boundary—violently inducing branch birth—and hence can serve as possible models for an object part coming into view. Again, such creations will be related to ligature.

A Proof of Theorem 1

Here we carry out detailed derivations leading to Theorem 1. From Fig. 2, observe that

$$Q - C_i = rN_i. \tag{16}$$

Taking the norm-squared of both sides of (16), we obtain

$$(Q - C_i) \cdot (Q - C_i) = |Q - C_i|^2 = r^2 |N_i|^2 = r^2, \tag{17}$$

and taking the time derivative (denoted $\dot{Q} = \frac{\partial Q}{\partial t}$), we get:

$$2(Q - C_i) \cdot (\dot{Q} - \dot{C}_i) = 2r\dot{r}. \tag{18}$$

Substituting (16), (2), and (1) into (18) and then simplifying, we obtain the pair of equations (for $i = 1, 2$):

$$\dot{r} = \tau N_i \cdot T + \nu N_i \cdot N - \nu_i. \tag{19}$$

Observe in Fig. 2 that:

$$N_i \cdot T = \cos\varphi, \quad N_i \cdot N = \mp \sin\varphi, \tag{20}$$

using the sign convention introduced in §3. Substituting, we get $\dot{r} = \tau \cos\varphi \mp \nu \sin\varphi - \nu_i$. By subtracting this equation for $i = 1$ from that for $i = 2$, we conclude: $\nu = \frac{\nu_2 - \nu_1}{2 \sin\varphi}$.

To compute the widening $\dot{\varphi}$, or rate of increase of the angle between N_i and T, we take the time derivative of $\cos\varphi = N_i \cdot T$ and see that:

$$-\dot{\varphi} \sin\varphi = \dot{N}_i \cdot T + N_i \cdot \dot{T}. \tag{21}$$

Now letting the orientation of T and T_i be θ and θ_i, respectively, note that:

$$\dot{T} = \frac{\partial}{\partial t}(\cos\theta, \sin\theta) = \dot{\theta}(-\sin\theta, \cos\theta) = \dot{\theta} N. \tag{22}$$

Symbol	*Description*
$' = \frac{\partial}{\partial s}$	derivative with respect to skeleton arc-length
$\dot{Q} = \frac{\partial Q}{\partial t}$	time derivative of skeleton
ν_i	boundary motion
κ	skeleton curvature
κ_i	boundary curvature
φ	angle between boundary normal and skeleton tangent
$C_i = C(s_i, t)$	boundary point
$g_i = \mp\frac{\partial s_i}{\partial s}$	boundary-axis ratio along boundary at C_i
N	normal to skeleton at Q
N_i	(inward) normal to boundary at C_i
Q	skeleton point
r	radius of maximal disc
s	skeleton arc-length
s_i	boundary arc-length
t	evolutionary time
T	skeleton tangent
$T_i = \frac{\partial C_i}{\partial s_i}$	boundary tangent
ν	velocity of skeleton in normal direction
τ	velocity of skeleton in tangential direction

Table 1: Glossary

Similarly,

$$\dot{N} = -\dot{\theta}T, \quad \dot{T}_i = \dot{\theta}_i N_i, \quad \dot{N}_i = -\dot{\theta}_i T_i. \tag{23}$$

Substituting (22) and (23) into (21), and noting $T_i \cdot T = N_i \cdot N$, we get: $-\dot{\varphi}\sin\varphi = -\dot{\theta}_i T_i \cdot T + N_i \cdot \dot{\theta} N = \pm\dot{\theta}_i \sin\varphi \mp \dot{\theta}\sin\varphi$, or: $\dot{\varphi} = \pm(\dot{\theta} - \dot{\theta}_i)$. Adding and subtracting these two equations, we obtain:

$$\dot{\varphi} = \frac{\dot{\theta}_2 - \dot{\theta}_1}{2}, \quad \dot{\theta} = \frac{\dot{\theta}_1 + \dot{\theta}_2}{2}. \tag{24}$$

To solve for $\dot{\theta}_i$, we shall proceed by performing an alternative derivation of $\dot{T}_i = \frac{\partial}{\partial t}\frac{\partial C_i}{\partial s_i}$. This requires that we study s_i and its derivatives. To ensure that the arc-length parameter s_i runs counter-clockwise along the boundary, we note:

$$s_i = \mp\int_0^s |C_i'(\sigma)| d\sigma,$$

and so we define the boundary-axis ratio [3] along the boundary at C_i as:

$$g_i := \mp\frac{\partial s_i}{\partial s} = +|C_i'| > 0. \tag{25}$$

To compute the time derivative of the boundary-axis ratio, observe that: $\frac{\partial g_i^2}{\partial t} = 2C_i' \cdot \dot{C}_i' = \mp 2 g_i T_i \cdot (\nu_i N_i)' = \mp 2 g_i T_i \cdot (\nu_i' N_i + \nu_i N_i') = \mp 2 g_i \nu_i T_i \cdot N_i'$.

The classical Frenet formulas [5] express arc-length derivatives of the local coordinate frame in terms of the local coordinate frame. For the skeleton, these formulas are:

$$T' = \kappa N, \quad N' = -\kappa T,$$

and for the boundary at C_i:

$$\frac{\partial T_i}{\partial s_i} = \kappa_i N_i, \quad \frac{\partial N_i}{\partial s_i} = -\kappa_i T_i.$$

Now $N_i' = \frac{\partial N_i}{\partial s_i}\frac{\partial s_i}{\partial s} = \pm\kappa_i g_i T_i$, and thus $\frac{\partial g_i^2}{\partial t} = -2\kappa_i g_i^2 \nu_i$. But, by the chain rule, $\frac{\partial g_i^2}{\partial t} = 2 g_i \dot{g}_i$, and so

$$\dot{g}_i = -\kappa_i g_i \nu_i. \tag{26}$$

Following [9] and using (26) and (25), we compute $\frac{\partial}{\partial t}\frac{\partial}{\partial s_i} = \frac{\partial}{\partial t}\frac{\partial s}{\partial s_i}\frac{\partial}{\partial s} = \mp\frac{\partial}{\partial t}(\frac{1}{g_i}\frac{\partial}{\partial s}) = \mp(-\frac{\dot{g}_i}{g_i^2}\frac{\partial}{\partial s} \mp \frac{1}{g_i}\frac{\partial}{\partial t}\frac{\partial}{\partial s}) = -\frac{-\kappa_i g_i \nu_i}{g_i}(\mp\frac{1}{g_i})\frac{\partial}{\partial s} \mp \frac{1}{g_i}\frac{\partial}{\partial s}\frac{\partial}{\partial t}$, or:

$$\frac{\partial}{\partial t}\frac{\partial}{\partial s_i} = \kappa_i \nu_i \frac{\partial}{\partial s_i} + \frac{\partial}{\partial s_i}\frac{\partial}{\partial t}. \tag{27}$$

Using this result, we find: $\dot{T}_i = \frac{\partial}{\partial t}\frac{\partial C_i}{\partial s_i} = \kappa_i \nu_i \frac{\partial C_i}{\partial s_i} + \frac{\partial \dot{C}_i}{\partial s_i} = \kappa_i \nu_i T_i + \frac{\partial \nu_i}{\partial s_i} N_i - \kappa_i \nu_i T_i$, or

$$\dot{T}_i = \frac{\partial \nu_i}{\partial s_i} N_i.$$

Comparing with (23), we get:

$$\dot{\theta}_i = \frac{\partial \nu_i}{\partial s_i}. \tag{28}$$

Substituting $\dot{\theta}_i$ into (24), we conclude:

$$\dot{\varphi} = \frac{\frac{\partial \nu_2}{\partial s_2} - \frac{\partial \nu_1}{\partial s_1}}{2}, \quad \dot{\theta} = \frac{\frac{\partial \nu_1}{\partial s_1} + \frac{\partial \nu_2}{\partial s_2}}{2}. \tag{29}$$

To compute the growth $\dot{r}$ of the radius of the maximal disc, we move all terms of (16) to the left and take the time derivative: $\dot{Q} - \dot{C}_i - \dot{r}N_i - r\dot{N}_i = 0$. Now we substitute in (2), (1), (23), and (28):

$$\tau T + \nu N - \nu_i N_i - \dot{r} N_i + r\frac{\partial \nu_i}{\partial s_i} T_i = 0. \tag{30}$$

After taking the dot product with N and making substitutions, we get the following two equations: $\nu \pm \nu_i \sin\varphi \pm \dot{r}\sin\varphi - r\frac{\partial \nu_i}{\partial s_i}\cos\varphi = 0$. We subtract the second equation from the first: $(\nu_1 + \nu_2)\sin\varphi + 2\dot{r}\sin\varphi + r(\frac{\partial \nu_2}{\partial s_2} - \frac{\partial \nu_1}{\partial s_1})\cos\varphi = 0$, and conclude:

$$\dot{r} = -r\dot{\varphi}\cot\varphi - \frac{\nu_1 + \nu_2}{2}. \tag{31}$$

To compute the tangential motion τ, we take the dot product of (30) with T and obtain after substitutions these two equations: $\tau - \nu_i \cos\varphi - \dot{r}\cos\varphi \mp r\frac{\partial \nu_i}{\partial s_i}\sin\varphi = 0$. After adding them, solving for τ, substituting for $\dot{r}$, and using (29), we conclude: $\tau = \frac{r}{2}(\frac{\partial \nu_2}{\partial s_2} - \frac{\partial \nu_1}{\partial s_1})(\cot\varphi\cos\varphi + \sin\varphi) = -\frac{r\dot{\varphi}}{\sin\varphi}$. Theorem 1 follows.

B Proof of Corollary 2

We would like to express the normal motion of the skeleton as a function of its curvature. We first take the derivative of $\cos\varphi = N_i \cdot T$ with respect to the arc-length along the skeleton: $-\varphi' \sin\varphi = N_i' \cdot T + N_i \cdot T' = \mp g_i \frac{\partial N_i}{\partial s_i} \cdot T + N_i \cdot \frac{\partial T}{\partial s} = \pm\kappa_i g_i T_i \cdot T + \kappa N_i \cdot N = -\kappa_i g_i \sin\varphi \mp \kappa \sin\varphi$, or $\varphi' = \kappa_i g_i \pm \kappa$. Subtracting these equations, we find:

$$\kappa = \frac{\kappa_2 g_2 - \kappa_1 g_1}{2}. \tag{32}$$

A straightforward way of computing g_i begins with the skeleton arc-length derivative of $C_i = Q - rN_i$, or:

$$C_i' = Q' - r'N_i - rN_i'. \tag{33}$$

To find r', we take the skeleton arc-length derivative of (17): $2rr' = 2(Q - C_i) \cdot (Q' - C_i') = 2rN_i \cdot (T \pm g_i T_i) = 2r\cos\varphi$, or, $r' = \cos\varphi$. We then substitute this into (33) and take the norm-squared, recalling the definition of g_i: $g_i^2 = |C_i|^2 = (T - \cos\varphi N_i \mp r\kappa_i g_i T_i)^2 = \sin^2\varphi + 2r\kappa_i g_i \sin\varphi + r^2\kappa_i^2 g_i^2 = (\sin\varphi + r\kappa_i g_i)^2$. Since $g_i > 0$, we obtain:

$$g_i = \frac{\sin\varphi}{1 - r\kappa_i}. \tag{34}$$

Substituting into (32), we see: $\kappa = \frac{\sin\varphi}{2}(\frac{\kappa_2}{1-r\kappa_2} - \frac{\kappa_1}{1-r\kappa 1}) = \frac{\sin\varphi}{2(1-r\kappa_1)(1-r\kappa_2)}(\kappa_2 - \kappa_1) = g_1 g_2 \frac{\kappa_2 - \kappa_1}{2\sin\varphi}$.Corollary 2 follows.

Acknowledgements

We thank Patrick Huggins, Martin Jägersand and especially Kaleem Siddiqi for helpful discussions. We also gratefully acknowledge the support of NSF ECS-9700588, NSF-LIS, AFOSR AF/F49620-98-1-0168, ARO DAAG55-98-1-0169, and MURI Grant.

References

[1] S. Angenent, "The zero set of a solution of a parabolic equation," *Journal für die reine und angewandte Mathematik* **390** (1988), pp. 79–96.

[2] J. August, K. Siddiqi and S. Zucker, "Ligature instabilities and the perceptual organization of shape," *Proc. CVPR* (1999), vol. 2, pp. 42–48.

[3] H. Blum and R. Nagel, "Shape description using weighted symmetric axis features," *Patt. Recogn.* **10** (1978), pp. 167–180.

[4] J. Bruce and P. Giblin, "Growth, motion and 1-parameter families of symmetry sets," *Proc. Royal Soc. Edinburgh* **104A** (1986), pp. 179-204.

[5] M. P. Do Carmo, *Differential Geometry of Curves and Surfaces,* Prentice-Hall, 1976.

[6] C. L. Epstein and M. Gage, "The curve shortening flow," in *Wave Motion: Theory, Modeling, and Computation*, A. Chorin and A. Majda, Eds., Springer, 1987.

[7] P. Giblin and B. B. Kimia, "On the Intrinsic Reconstruction of Shape from its Symmetries," *Proc. CVPR* (1999), pp. 79–84.

[8] M. Grayson, "The heat equation shrinks embedded plane curves to round points," *J. Differential Geometry* **26** (1987), pp. 285-314.

[9] B. B. Kimia, A. Tannenbaum, and S. W. Zucker, "On the evolution of curves via a function of curvature, I: the classical case," *J. Math. Anal. and Appl.* **163** (1992), pp. 438-458.

[10] B. B. Kimia, A. Tannenbaum, and S. W. Zucker, "Shapes, shocks, and deformations, I: the components of shape and the reaction-diffusion space," *Intl. J. Computer Vision* **15** (1995), pp. 189-224.

[11] J. Koenderink, *Solid Shape*, MIT Press, 1990.

[12] T. Körner, *Fourier Analysis*, Cambridge U. Press, 1988.

[13] H. Matano, "Nonincrease of the lap number of a solution for a one-dimensional semi-linear parabolic equation," *J. Fac. Sci. Univ. Tokyo* **29** (1982), pp. 401-441.

[14] U. Montanari, "A Method for Obtaining Skeletons Using a Quasi-Euclidean Distance," *J. Assoc. Comput. Machinery*, **15** (1968), pp. 600–624.

[15] R. L. Ogniewicz and O. Kübler, "Hierarchic Voronoi skeletons", *Patt. Recogn.* **28** (1995), pp. 343–359.

[16] D. Shaked, *Symmetry, Invariance, and Evolution in Planar Shape Analysis*, Ph.D. thesis, Technion, 1996.

[17] K. Siddiqi, A. Shokoufandeh, S. Dickinson and S. Zucker, "Shock Graphs and Shape Matching", *Proc. ICCV* (1998), pp. 222–229.

[18] R. Taxiera, *Curvature Motions, Medial Axes and Distance Transforms*, Ph.D. thesis, Harvard U., 1998.

[19] Y. Yomdin, "On the local structure of a generic central set," *Compositio Mathematica* **43** (1981), pp. 225-238.

[20] S.C. Zhu, "Stochastic Computation of Medial Axis in Markov Random Fields," *Proc. CVPR* (1998), pp. 72–79.